



a264570

AEOSR-TR- 88 0047

2

# IMPROVED GALLIUM NITRIDE AND ALUMINUM NITRIDE ELECTRONIC MATERIALS

W. D. Partlow (PI), W. J. Choyke, R. P. Devaty,  
John T. Yates, Jr., Karl-Heinz Bornschauer,  
P. J. Chen, C. C. Cheng, M. L. Colaianni, H. Gutleben,  
S. R. Lucas, M. F. MacMillan

Annual Report for the period  
February 20, 1992 to February 19, 1993

General Order No. 1 WGD-12523-CE

Contract No. F49620-91-C-0032

Air Force Office of Scientific Research  
Bolling Air Force Base  
Washington, DC 20332

March 25, 1993

**S** DTIC **D**  
ELECTE  
MAY 26 1993  
**A**

AIR FORCE OFFICE OF SCIENTIFIC RESEARCH (AFOSR)  
NOTICE OF CONTRACT AWARD  
THIS CONTRACT IS FOR THE  
PURCHASE OF ELECTRONIC  
MATERIALS  
DIRECTOR  
STAFF PROGRAM MANAGER  
AFOSR-12  
and is

This document has been approved  
for public release and sale; its  
distribution is unlimited.

93 5 25 039

93-11595



45992



Westinghouse STC  
1310 Beulah Road  
Pittsburgh, Pennsylvania 15235-5098

**IMPROVED GALLIUM NITRIDE  
AND ALUMINUM NITRIDE  
ELECTRONIC MATERIALS**

W. D. Partlow (PI), W. J. Choyke, R. P. Devaty,  
John T. Yates, Jr., Karl-Heinz Bornschauer,  
P. J. Chen, C. C. Cheng, M. L. Colaianni, H. Gutleben,  
S. R. Lucas, M. F. MacMillan

Annual Report for the period  
February 20, 1992 to February 19, 1993

General Order No. I WGD-12523-CE

Contract No. F49620-91-C-0032

Air Force Office of Scientific Research  
Bolling Air Force Base  
Washington, DC 20332

March 25, 1993



Westinghouse STC  
1310 Beulah Road  
Pittsburgh, Pennsylvania 15235-5098

# REPORT DOCUMENTATION PAGE

*Form Approved*  
OMB No. 0704-0188

Public reporting burden for this collection of information is estimated to average 1 hour per response, including the time for reviewing instructions, searching existing data sources, gathering and maintaining the data needed, and completing and reviewing the collection of information. Send comments regarding this burden estimate or any other aspect of this collection of information, including suggestions for reducing this burden, to Washington Headquarters Services, Directorate for Information Operations and Reports, 1215 Jefferson Davis Highway, Suite 1204, Arlington, VA 22202-4302, and to the Office of Management and Budget, Paperwork Reduction Project (0704-0188), Washington, DC 20503.

<b>1. AGENCY USE ONLY (Leave blank)</b>		<b>2. REPORT DATE</b>	<b>3. REPORT TYPE AND DATES COVERED</b> Annual Feb. 20, 1992 - Feb. 19, 1993	
<b>4. TITLE AND SUBTITLE</b> IMPROVED GALLIUM NITRIDE AND ALUMINUM NITRIDE ELECTRONIC MATERIALS			<b>5. FUNDING NUMBERS</b>  F49620-91-C-0032	
<b>6. AUTHOR(S)</b> W. D. Partlow (PI), W. J. Choyke, R. P. Devaty, John T. Yates, Jr., Karl-Heinz Bornschauer, P. J. Chen, C. C. Cheng, M. L. Colaianni, H. Gutleben, S. R. Lucas, M. F. MacMillan				
<b>7. PERFORMING ORGANIZATION NAME(S) AND ADDRESS(ES)</b> Westinghouse STC 1310 Beulah Road Pittsburgh, PA 15235-5098			<b>8. PERFORMING ORGANIZATION REPORT NUMBER</b>  93-9SB2-ALGAN-R1	
<b>9. SPONSORING/MONITORING AGENCY NAME(S) AND ADDRESS(ES)</b>  Air Force Office of Scientific Research <i>ME</i> Bolling Air Force Base Washington, DC 20332			<b>10. SPONSORING/MONITORING AGENCY REPORT NUMBER</b>  <i>2305 ES</i>	
<b>11. SUPPLEMENTARY NOTES</b>				
<b>11a. DISTRIBUTION/AVAILABILITY STATEMENT</b>  <i>Unlimited</i>			<b>11b. DISTRIBUTION CODE</b>	
<b>13. ABSTRACT (Maximum 200 words)</b>  This report describes the progress in the second year of a three year program to improve the quality of gallium and aluminum nitride electronic materials. In this period we completed surface chemistry equipment modifications and characterization, and began experiments to control and understand the surface reactions associated with the growth of gallium nitride. By subjecting a physisorbed monolayer of trimethyl gallium (TMG) to a cool beam of atomic hydrogen atoms, we successfully converted it to metallic Ga, which is much more reactive with nitriding species, and will result in a more stoichiometric and higher purity gallium nitride. In the materials characterization effort of the program, infrared reflectance spectral and cathodoluminescence spectra were measured for epitaxial AlN films. The reflectance spectra were compared to a Lorentz oscillator model which make it possible to separate out the contribution of the AlN even when the bands of the film and substrate overlapped.				
<b>14. SUBJECT TERMS</b>			<b>15. NUMBER OF PAGES</b> 41	
			<b>16. PRICE CODE</b>	
<b>17. SECURITY CLASSIFICATION OF REPORT</b>  Unrestricted	<b>18. SECURITY CLASSIFICATION OF THIS PAGE</b>  Unrestricted	<b>19. SECURITY CLASSIFICATION OF ABSTRACT</b>  Unrestricted	<b>20. LIMITATION OF ABSTRACT</b>	

# IMPROVED GALLIUM NITRIDE AND ALUMINUM NITRIDE ELECTRONIC MATERIALS

W. D. Partlow (P. I.), W. J. Choyke, R. P. Devaty,  
John T. Yates, Jr., K.-H. Bornscheuer, P. J. Chen, C. C. Cheng,  
M. L. Colaianni, H. Gutleben, S. R. Lucas, M. F. MacMillan

## ABSTRACT

This report describes the progress in the second year of a three year program to improve the quality of gallium and aluminum nitride electronic materials. In this period we completed surface chemistry equipment modifications and characterization, and began experiments to control and understand the surface reactions associated with the growth of gallium nitride. By subjecting a physisorbed monolayer of trimethyl gallium (TMG) to a cool beam of atomic hydrogen atoms, we successfully converted it to metallic Ga, which is much more reactive with nitriding species, and will result in a more stoichiometric and higher purity gallium nitride. In the materials characterization effort of the program, infrared reflectance spectra and cathodoluminescence spectra were measured for epitaxial AlN films. The reflectance spectra were compared to a Lorentz oscillator model which made it possible to separate out the contribution of the AlN even when the bands of the film and substrate overlapped.

Accession For	
NTIS	CRA&I
DTIC	FAS
Unannounced	CS
Justification	
By	
Distribution	
Availability Codes	
Dist	Availability for special
A-1	

## 1. OVERVIEW AND STATUS

The program approaches its objective of improving the electronic quality of Group III nitrides from two directions: (a) understanding and improving the fundamental deposition steps in the material growth through surface chemistry experiments; and (b) applying relevant characterization techniques to epitaxial layers, developing new characterization tools needed for understanding and evaluating the material quality.

The surface chemistry experiments have concentrated on the use of atomic hydrogen to activate adsorbed organometallic surface layers. These layers serve as reaction precursors for nitride formation, and in the past have not fully reacted in deposition processes. This resulted in a nitrogen deficiency in the epitaxial layers, and in the incorporation of carbon which was retained from these reaction precursors. In order to carry out our experiments it was necessary to design, build, and characterize a new type of atomic hydrogen source. The source uses a cryogenically cooled surface to reflect the atomic-H beam to the growth surface, while eliminating almost all substrate heating from the hot filament that is used to generate the atomic-H from the dissociation of molecular hydrogen. The unwanted radiation had made it impossible utilize atomic hydrogen without thermally decomposing the layer of organometallic precursor. The source successfully provides a cleaner, more intense atomic H beam than competitive techniques such as plasmas, and it is likely to find uses many areas of surface treatment and activation. The details of the atomic hydrogen source and its characteristics are described in a publication<sup>1</sup> which is included in the Appendix 1 of this report. We have applied for a patent on the cooled atomic hydrogen source.

In Section 2 we describe experiments that successfully demonstrate the use of atomic hydrogen to chemically activate adsorbed trimethyl gallium, essentially removing the carbon from the organometallic precursor. We believe that this new process developed on this program has broad implications in the improvement of electronic materials quality. In the third and final year of the program we plan to follow-up these results with demonstrations of the use of atomic-H activation to synthesize improved materials.

Materials characterization experiments consisted of cathodoluminescence measurements of the electronic properties of the nitride layers, and infrared reflectance measurements which provided insight into their structural properties. Although we continued our collaborations on cathodoluminescence characterization of nitrides with nine laboratories around the world<sup>2</sup>, most of the effort in this reporting period was concentrated in the development of a Lorentz oscillator model of the infrared reflectance of AlN layers on substrates such as SiC and Si. The model takes into account film and substrate anisotropy and non-normal incidence. Comparison of infrared reflectance measurements to the model provides information on the thickness, orientation, and quality of epitaxial AlN films. The results of this study are contained in a publication<sup>3</sup>, which is included as Appendix 2 of this report.

Work has also begun on a vacuum ultraviolet reflectance spectrometer, which will be put into use on the third year of this program to obtain new information on the band structure of the Group III nitrides.

## 2. CHEMISTRY OF ADSORBED LAYERS OF TRIMETHYL GALLIUM

### A. Objective And Approach

To understand and control the steps in producing GaN from trimethyl gallium (TMG) on an atomically clean surface, we characterized the behavior of adsorbed layers of TMG by thermal desorption studies, backed up by Auger measurements of the surfaces. Adsorbed TMG layers on hydrogen-passivated Si(100) and on SiO<sub>2</sub>-coated Si(100) surfaces have been subjected to a beam of atomic hydrogen with the objective of removing CH<sub>3</sub> groups by reaction at low temperatures.

### B. Results

We began by using the Si(100), passivated by an atomic H beam, as a substrate. Since TMG adsorbs only very weakly on the passivated Si(100) by physisorption, studies of this TMG layer provide information about the TMG molecule in the most unperturbed state that can be obtained on a surface. Through a combination of thermal desorption and Auger spectroscopic measurements, we have shown that the TMG molecule is strongly reactive at 108 K with atomic H. One or more of the CH<sub>3</sub> groups disappear at 108 K from the weakly-bound TMG molecule.

The dependence of the desorption characteristics of TMG and its products on atomic hydrogen activation is easily seen in Fig. 1, which plots the mass spectroscopy ion current of the Ga<sup>+</sup> (mass 69) versus temperature for several different exposures of the adsorbed TMG layer to atomic-H. Up to 1800 monolayers of atomic-H were used. The unactivated TMG layer, shown in the lower trace, desorbs in a narrow temperature range at about 125K. Treatment of the layer with atomic-H eliminates this peak entirely, reducing the height of the 125K peak, and shifting the desorption into broader peaks at higher temperatures extending up to

Desorption Mass Spectra for TMG following Atomic Hydrogen Exposure –  $T_s = 108$  K

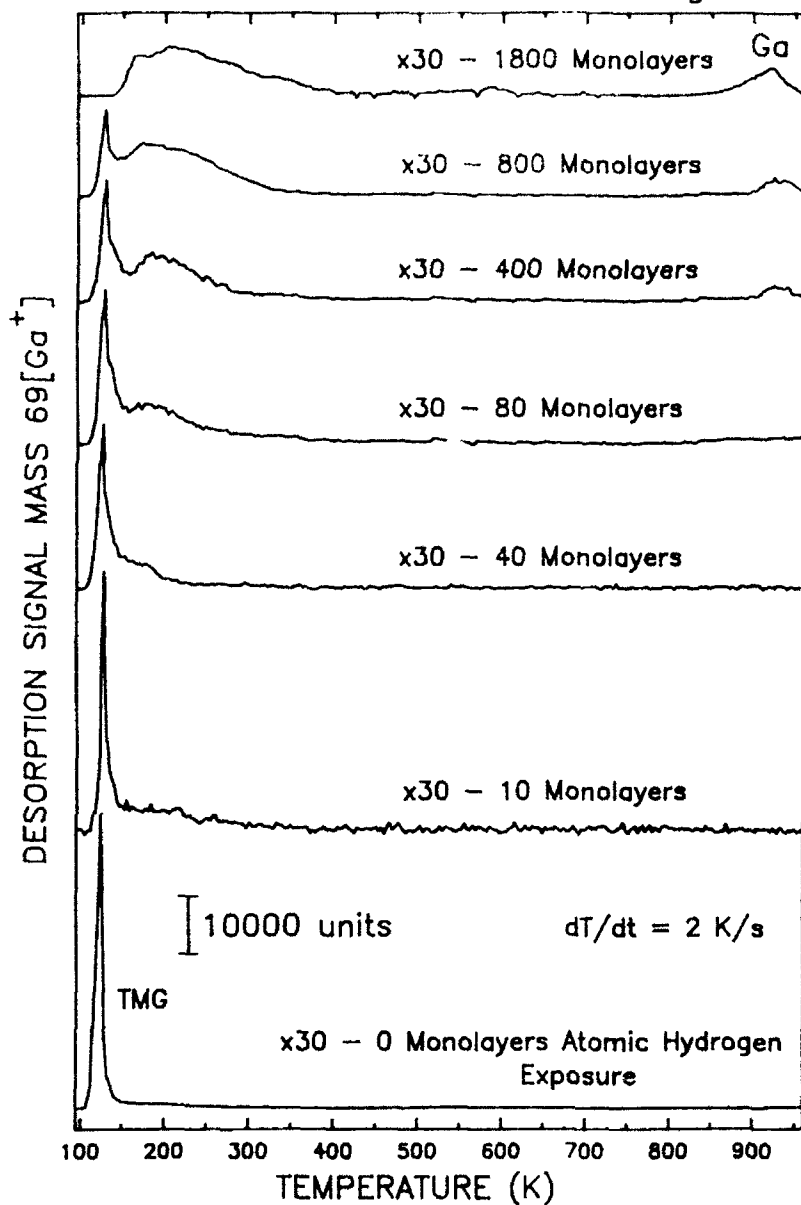


Fig. 1. Mass spectroscopy ion current of the  $\text{Ga}^+$  (mass 69) versus temperature for several different exposures of the adsorbed TMG layer to atomic-H, showing change in character of the desorption spectra of the transformed layer.

400K. These broad peaks indicate that the TMG has been converted to different species such as  $\text{Ga}(\text{CH}_3)_2$  or  $\text{Ga}(\text{CH}_3)$ , which bond more strongly to the Si(100) surface. At high H exposures the metallic Ga desorption peak at 925K can be seen. Traces of the other mass fragments of TMG confirm the modification of TMG, and reveal more details of the changes. The desorption spectra of the TMG parent peak (mass 114) is shown in Fig. 2, revealing that the narrow desorption peak at 125K is shifted to slightly higher temperatures under exposure of up to eight monolayers of atomic-H, and that this peak is essentially eliminated after exposure to 80 monolayers of atomic-H.

The surface modifications indicated in Fig. 1 and Fig. 2 are slow at the surface temperature used for the atomic-H reactions, and the loss of  $\text{CH}_3$  groups is incomplete at 108 K. We sought to find ways to speed up the process, and drive it to completion. This was achieved by adsorbing TMG as a more strongly bound surface molecule on a  $\text{SiO}_2/\text{Si}(100)$  surface, which has a coating of about  $30\text{\AA}$  of  $\text{SiO}_2$ . This made it possible to work at higher surface temperatures during the atomic-H activation, and therefore to increase the rate of surface reactions. These experiments at 138 K have proven to be highly successful: COMPLETE REMOVAL OF  $\text{CH}_3$  GROUPS CAN BE ACHIEVED BY RELATIVELY LOW LEVELS OF ATOMIC-H ACTIVATION. The key result that demonstrates this process is shown in Fig. 3, where Auger spectroscopy has been used to measure the departure of most of the carbon atoms from the adsorbed layer through the decrease in Auger signal (along with an increase in Ga signal that has not been fully explained). The small amount of carbon remaining has a different lineshape from the methyl carbon, and is probably associated with defects or experimental contamination. This experiment clearly shows that the methyl removal by atomic-H occurs efficiently at low temperatures. A NEW TYPE OF LOW TEMPERATURE ACTIVATION OF ADSORBED ORGANOMETALLIC MOLECULES HAS BEEN DISCOVERED IN THESE EXPERIMENTS. The overall reaction is schematically represented in Fig. 4 (which was used as Fig. 3.5 of the original proposal for this research).

Desorption Mass Spectra following  
Atomic Hydrogen Exposure –  $T_s = 108$  K

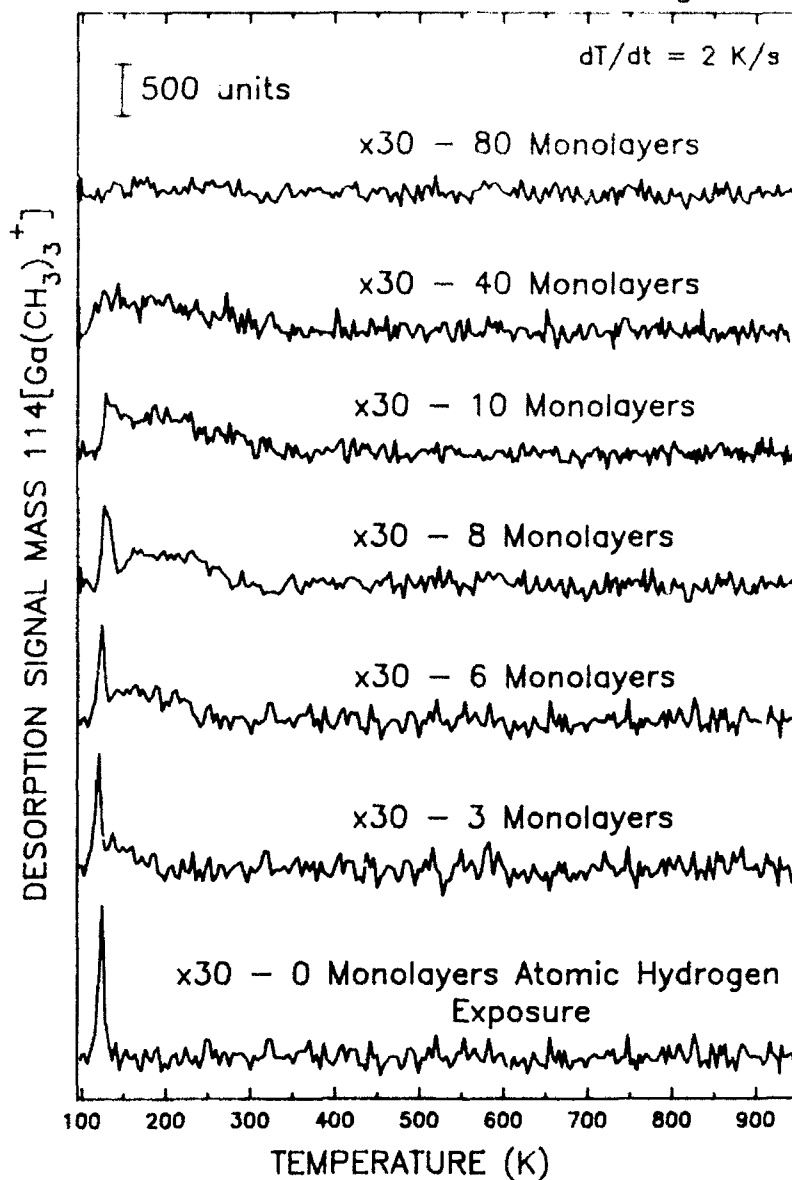


Fig. 2. The desorption spectra of the TMG parent peak (mass 114), revealing that the narrow desorption peak at 125K is shifted to slightly higher temperatures under exposure of up to eight monolayers of atomic-H, and that this peak is essentially eliminated after exposure to 80 monolayers of atomic-H.

Auger Measurements of the Extraction of  $\text{CH}_3$  Groups from TMG on  $\text{SiO}_2$  by Atomic Hydrogen -  $T_s = 138 \text{ K}$

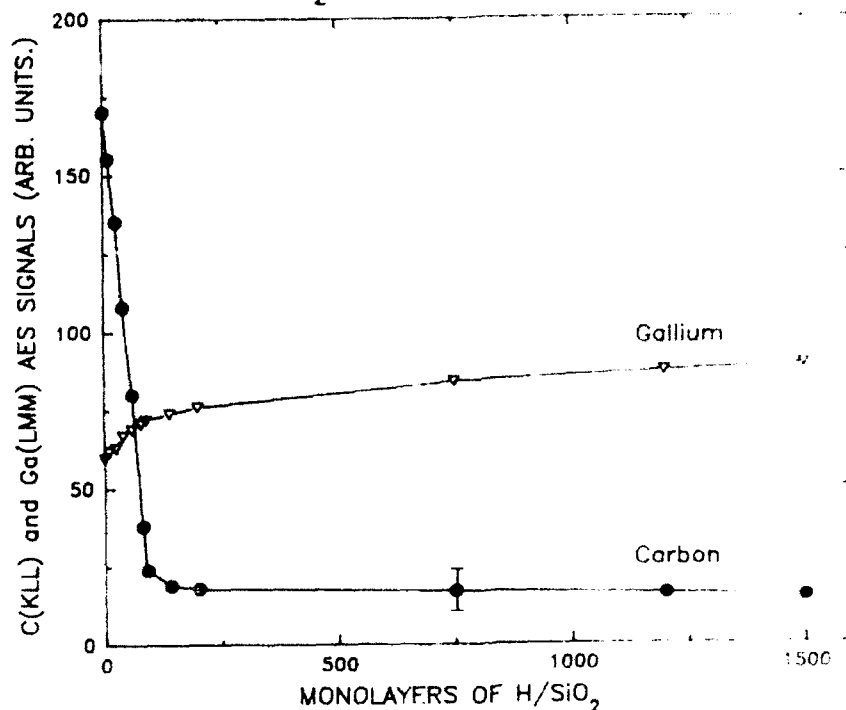


Fig. 3. Auger studies of the effect of atomic-H on TMG adsorbed on  $\text{SiO}_2/\text{Si}(100)$  at  $T=138 \text{ K}$ . The carbon Auger signal is reduced to a low background level which is not associated with the methyl radical.

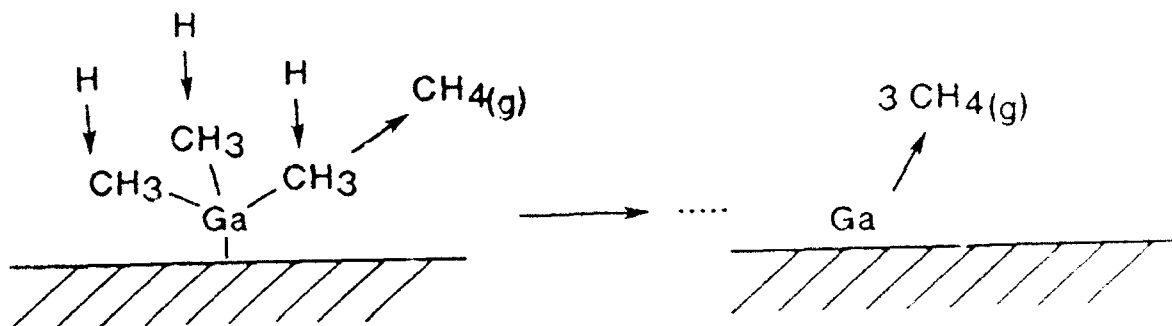


Fig. 4. Schematic of the elimination of  $\text{CH}_3$  ligands with a beam of H atoms, leading to a pure Ga layer without carbon.

### C. Implications of the Research

The results obtained for the new atomic-H-induced reaction have significant implications in semiconductor film growth which extend far beyond the Ga(CH<sub>3</sub>)<sub>3</sub> system. With regard to GaN and AlN growth, these results indicate that an atomic-H beam added to a metalorganic molecular beam epitaxy (MOMBE) process will increase the reactivity of the adsorbed organometallic precursors and will lead to more complete reaction with the nitriding beam. Fewer nitrogen vacancies and lower carbon impurities are expected. Similar improvements are expected for atomic layer epitaxy (ALE) processes, where the atomic-H beam makes it possible for the first time to have a "Type 1" ALE process for Ga, which also uses the advantages of an active metal surface reaction rather than an exchange reaction with adsorbed organometallic precursors.

Some broader implications of these results are:

1. The demonstrated surface activation of organometallic molecules by ligand removal with atomic-H is very likely to stimulate the use of atomic-H activation in many semiconductor processes where thermodynamically stable hydrogenated leaving groups may be produced.
2. The efficient removal of carbon atoms in organometallic precursors by atomic-H activation will likely expand the applicability of organometallic for the synthesis of ultra-pure materials.
3. The ligand removal by atomic-H applies to the gas phase as well as to surface-bound molecules. Thus, there are implications for the control of the composition of gas phase reaction streams by adjustment of the atomic hydrogen concentration.

4. The new atomic-H chemistry may be carried out at CRYOGENIC temperatures, offering significant possibilities for dramatically lowering the temperature of film growth from organometallic precursors.

### 3. REFERENCES

1. K. H. Bornscheuer, S. R. Lucas, W. J. Choyke, W. D. Partlow, and J. T. Yates, Jr., "Reflector Atomic Hydrogen Source- A Method For Producing Pure Atomic Hydrogen In Ultrahigh Vacuum", to be published, *Journal of Vacuum Science and Technology* 11, Sept/Oct, 1993.
2. Khan, M. A. K., Kuznia, J. N. Skogman, R. A., Olson, D. T., MacMillan, M., Choyke, W. J., Low pressure metalorganic chemical vapor deposition of AlN over sapphire substrates, *Appl. Phys. Lett.* (accepted) 1993.
3. M. F. MacMillan, R. P. Devaty, and W. J. Choyke, "Infrared Reflectance of Thin Aluminum Nitride Films on Various Substrates", *Applied Physics Letters* 62, 750 (1993).

## **APPENDIX 1:**

K. H. Bornscheuer, S. R. Lucas, W. J. Choyke, W. D. Partlow, and J. T. Yates, Jr., "Reflector Atomic Hydrogen Source- A Method For Producing Pure Atomic Hydrogen In Ultrahigh Vacuum", to be published, *Journal of Vacuum Science and Technology* 11, Sept/Oct, 1993.

Submitted to: Journal of Vacuum  
Science and Technology

Date: November 25, 1992

Reflector Atomic Hydrogen Source-A Method For Producing Pure Atomic  
Hydrogen In Ultrahigh Vacuum

K.H. Bornscheuer,<sup>†</sup> S.R. Lucas, W.J. Choyke,<sup>††</sup> W.D. Partlow <sup>†††</sup>  
and J.T. Yates, Jr.

Surface Science Center  
Department of Chemistry  
University of Pittsburgh  
Pittsburgh, PA 15260

<sup>†</sup> Department of Physics, University of Kassel

<sup>††</sup> Department of Physics, University of Pittsburgh

<sup>†††</sup> Westinghouse Science and Technology Center

# Reflector Atomic Hydrogen Source-A Method For Producing Pure Atomic Hydrogen In Ultrahigh Vacuum

K.H. Bornscheuer,<sup>†</sup> S.R. Lucas, W.J. Choyke,<sup>††</sup> W.D. Partlow<sup>†††</sup>  
and J.T. Yates, Jr.

Surface Science Center  
Department of Chemistry  
University of Pittsburgh  
Pittsburgh, PA 15260

## Abstract

A tungsten filament atomic hydrogen source placed in an effusive H<sub>2</sub> molecular beam has been combined with a cryogenically-cooled Pyrex reflector. This arrangement permits efficient production and transfer of atomic hydrogen to a sample surface by a non-line-of-sight route. The arrangement eliminates most radiation heating of the sample. A silicon(100) crystal sample was used in this study.

In addition, with the beam source, high local H<sub>2</sub> gas densities and atomic hydrogen production rates in the filament region may be achieved without producing excessive gas loads in an ultrahigh vacuum system. The indirect source protects the sample from possible metal contamination evolved from the hot tungsten filament, and efficiently delivers only atomic and molecular hydrogen species to the sample. The efficiency of this arrangement has been quantitatively compared to a line-of-sight filament source of atomic hydrogen.

# Reflector Atomic Hydrogen Source - A Method for Producing Pure Atomic Hydrogen in Ultrahigh Vacuum

K.H. Bornscheuer,<sup>†</sup> S.R. Lucas, W.J. Choyke,<sup>††</sup> W.D. Partlow<sup>†††</sup>  
and J.T. Yates, Jr.

Surface Science Center  
Department of Chemistry  
University of Pittsburgh  
Pittsburgh, PA 15260

## I. Introduction

Atomic hydrogen is a useful reactant for inducing surface chemistry on semiconductors and on metals. The high reactivity of atomic hydrogen can be ascribed to the 52.1 kcal/g. atom (2.26 eV) of additional potential energy which it carries compared to its energy in the  $H_2$  molecule. Many types of sources [1] of atomic hydrogen have been employed since Langmuir first produced atomic hydrogen on a hot tungsten filament [2,3]. These sources, which often involve electronic excitation processes, sometimes produces photons, ions, metastable species and gaseous impurities in addition to atomic hydrogen. In contrast, the hot tungsten filament source provides only atomic and molecular hydrogen. A disadvantage of the conventional hot tungsten filament H source is the production of radiation which will heat the sample exposed in a line-of-sight geometry to the filament. Thus, surface processes induced by atomic hydrogen bombardment may be influenced by the radiation heating effect of the filament on the surface receiving the atomic hydrogen. This paper presents a new method for transferring atomic hydrogen to a surface which avoids the majority of the heating effect due to radiation. This method also avoids possible contamination of the surface from the hot metal of the filament assembly. The efficiency of the new source is evaluated

using a Si(100) crystal as an integrating detector of the atomic hydrogen.

The production of atomic hydrogen on hot tungsten has been thoroughly investigated by a number of other workers [4-6]. It has been found that the efficiency of H atom production is proportional to  $(P_{H_2})^{1/2}$  at  $H_2$  pressures above  $\sim 10^{-6}$  Torr as surface conditions exist in pseudo-equilibrium with the gas phase. At lower  $H_2$  pressures, the H atom production rate is proportional to  $P_{H_2}$ . Under these conditions, the reported efficiency of  $H_2$  dissociation is  $\sim 0.3$  per  $H_2$  collision at temperatures above 2500 K [4]. It has been observed that the efficiency is decreased by impurities often present on a tungsten filament, and this decrease in dissociation efficiency is generally accompanied by a decrease in the activation energy for dissociation [5]. The reasons for this effect are currently unknown.

In this paper we employ a unique cryogenically-cooled reflector for atomic hydrogen which allows H atoms to reach a silicon single crystal only by an indirect route, eliminating the line-of-sight geometry and most of the radiation heating associated with this geometry. The efficiency of this arrangement has been evaluated and compared with a line-of-sight geometry.

## II. Experimental Details

Figure 1 shows a schematic diagram of the apparatus used in this work. The Si(100) crystal used as an integrating detector of atomic hydrogen may be placed in four positions for the experiments described here. In addition, it may be subjected to ion bombardment followed by annealing for cleaning, and to investigation by Auger spectroscopy using a single pass cylindrical mirror electron energy analyzer (not shown). The vacuum system also contains a reverse view LEED apparatus (not shown). The base pressure in this apparatus is  $5 \times 10^{-11}$

Torr. The vacuum system is pumped by a 270 L/s ion pump, a 150 L/s turbomolecular pump, and a titanium sublimation pump. For all studies of atomic hydrogen production, the turbomolecular pump is employed exclusively. For temperature programmed desorption studies only the turbomolecular pump and the ion pump were employed.

The primary atomic hydrogen source used here is shown at position 1. It consists of a 1.5 cm diameter flat spiral coil of 0.025 cm diameter tungsten wire with a wire length of 14.5 cm. This W coil is located at the exit position of an effusive dosing arrangement made of stainless steel. The W filament is shielded from direct line-of-sight exposure to the silicon crystal to avoid significant radiation heating effects. H<sub>2</sub> effuses from this doser source to the tungsten coil where a portion of the H<sub>2</sub> is converted to atomic H. The temperature of the W coil was measured by an optical pyrometer; in addition, its temperature can be accurately estimated from the electrical current used for heating using calibration tables of temperature versus current for tungsten wire of this diameter [7]. A fraction of the atomic hydrogen produced is incident on a Pyrex glass reflector plate which may be cooled by liquid nitrogen to a measured temperature of 120 K by filling a reservoir behind the plate with liquid nitrogen. Thermal contact between the back of the Pyrex plate and the reservoir is achieved using indium solder. A portion of the incident atomic hydrogen is reflected from the Pyrex plate and is intercepted by the crystal. An estimate, based on the geometry of the apparatus [8], indicates that the flux of atomic hydrogen from the H atom doser will be reduced by about a factor of four compared to the line-of-sight geometry. This calculation considers the solid angles subtended by the Pyrex plate and the crystal and assumes complete reflection of atomic H by the Pyrex plate. In this calculation, a cosine distribution of atomic hydrogen was assumed for the planar source and the planar reflector.

Hydrogen flow rates into the apparatus have been calibrated using a pinhole conductance limiter of known conductance, comparing the steady state H<sub>2</sub> pressure with the flow rate of H<sub>2</sub> into the pumped chamber [9]. These measurements showed that a hydrogen pressure of  $2.0 \times 10^{-7}$  Torr (corrected ion gauge) corresponded to a flow rate of  $2.15 \times 10^{16}$  H<sub>2</sub>/s. For these measurements, done with the titanium sublimation pump active, the effective system pumping speed is 3330 L/s for H<sub>2</sub>.

The Si(100)[B-doped, p-type, 10 ohm cm] crystal is 1.3 cm x 1.3 cm x 0.15 cm thick, and is heated resistively. Prior to insertion into the chamber, the crystal was cleaned with a hydrogen peroxide/HF(aq) modified RCA procedure [10]. The silicon crystal is mounted on Ta foil supports (0.0125 cm thick), two of which fit into 0.025 cm wide slots in opposing edges of the crystal. These Ta supports are welded to W support leads (0.14 cm diameter) which are in contact with a liquid nitrogen-cooled OFHC copper mounting assembly [11]. The temperature of the crystal is measured with a chromel/constantan thermocouple wedged into a third slot on the silicon crystal and protected from contact with the silicon by means of a double layer of Ta foil [11,12]. The crystal may be cooled to 100 K or heated to 1200 K using a temperature programmer. Final cleaning is achieved after Ar<sup>+</sup> bombardment (2 keV; 3.0 uA) by heating for 900 s at 1200 K. The clean Si(100) crystal exhibits a sharp (2 x 1) and (1 x 2) LEED pattern originating from orthogonal domains.

Auger spectroscopy was employed to ascertain that the atomic hydrogen sources in this work did not deliver impurities to the Si(100) surface. An Auger spectrum of the Si(100) crystal after exposure to atomic hydrogen and heating to desorb hydrogen is shown in Figure 2. The only detectable surface impurity of significance is sulfur and its estimated atomic fraction in the depth of Auger

sampling is 0.5%. It is noted that carbon, oxygen and tungsten in detectable surface concentrations are absent.

Since the H atom reflector apparatus has been designed to eliminate much of the radiation heating associated with a line-of-sight geometry, it was important to measure the amount of indirect radiation transfer to the crystal in position 1 during atomic hydrogen dosing. This is shown in Figure 3, where the crystal temperature is monitored as a function of time. For a W source temperature of 2000 K, the crystal temperature rises by about 17 K over a period of 500 seconds due to heating from the filament. The magnitude of the radiation heating effect will be related to the quality of the thermal contact between the crystal and its cooled support assembly.

Following the adsorption of atomic hydrogen in position 1, the crystal is rotated to the mass spectrometer (position 3) for line-of-sight thermal desorption measurements. The front surface of the crystal is reproducibly placed 0.2 cm from the 0.5 cm diameter aperture of the mass spectrometer. This aperture is biased at -100 V, to avoid emission of stray electrons from the mass spectrometer. The mass spectrometer sensitivity is measured before and after each hydrogen coverage measurement at two argon pressures, using the ionization gauge as a calibration standard, and all hydrogen coverages measured by temperature programmed desorption are corrected for mass spectrometer sensitivity changes.

The Si(100) crystal may also be subjected to atomic hydrogen exposure using line-of-sight geometry from a hot W filament source in position 2. The filament in this source is identical to that used in the effusive doser reflector source at position 1. The relative efficiencies of the two sources were measured using identical H<sub>2</sub> gas densities at both sources (by introducing H<sub>2</sub> as a random gas flux through a tube which is directed away from the H atom doser locations) and measuring the hydrogen coverage increase in both cases.

background species were made at position 4 with the ionization gauge operating. The measurements demonstrate that there may be a very small background atomic hydrogen adsorption effect due to the ionization gauge.

### III. Results

Figure 4 shows typical thermal desorption measurements made on Si(100) after exposure to atomic hydrogen from the reflector source (position 1) at a crystal temperature (maintained by electrical heating) of 400 K. This elevated temperature was selected in order to retard the production of silane which causes etching of the silicon [13]. The maximum surface coverage which can be reached at this crystal temperature is 1.33 H/Si, producing a (3x1) LEED pattern in agreement with other studies [13].

In accordance with previous measurements made in a number of laboratories [13,14], the H<sub>2</sub> desorption spectra exhibit, at lower hydrogen coverages, a monohydride feature desorbing with first-order kinetics with peak maximum near 770 K. The monohydride surface condition is associated with a (2 x 1) LEED pattern which converts to a (3 x 1) pattern at high H coverages. At higher hydrogen coverages, an additional dihydride desorption process occurs with a peak maximum at approximately 650 K. The integrated area of the desorption traces above background is proportional to the surface coverage of hydrogen on the Si(100).

Figure 5 shows the growth of the hydrogen coverage for increasing exposure to atomic hydrogen using the effusive doser reflector source. The curve is divided into two atomic hydrogen exposure regions corresponding to the evolution of the monohydride and the monohydride and dihydride desorption features. The coverage smoothly approaches an asymptotic limit of 1.33 H/Si

established by previous calibration measurements [13,15].

The efficiency of the hot tungsten source for the generation of atomic hydrogen was measured as a function of tungsten temperature using the reflector source and the crystal in position 1. The rate of atomic hydrogen production for various exposure times and for various H<sub>2</sub> flow rates through the effusive doser was measured using the coverage-vs-exposure curve of Figure 5 where all measurements were made in the initial uptake region which is nearly linear. Figure 6 shows that above a W filament temperature of about 2000 K, the efficiency of atomic hydrogen production reaches a plateau, and a further W temperature increase does not cause a higher rate of atomic hydrogen production.

Figure 7 shows the comparison of the rate of hydrogen coverage increase for the crystal in positions 1, 2, and 4. For the experiments shown here the hydrogen gas densities at the tungsten filaments (position 1 and position 2) are maintained at the same level by using random gas admission and a pressure of  $2 \times 10^{-7}$  Torr (corrected). The total hydrogen flow required to achieve a constant coverage in the two geometries is shown by the segments labeled F<sub>1</sub> and F<sub>2</sub>. The ratio  $\alpha = 4.8 \pm 0.3$  indicates that the H atom transfer efficiency of the line-of-sight atomic hydrogen source is 4.8 times as great as the reflector doser. The growth of the hydrogen coverage on the crystal in position 4 from very small background effects is shown by the lower curve of Figure 7. This background curve was obtained using an identical H<sub>2</sub> gas density as the other curves (corrected P<sub>H<sub>2</sub></sub> =  $2 \times 10^{-7}$  Torr), with the ionization gauge filament either on or off. Within the accuracy of measurement, the rate of adsorption of hydrogen is independent of whether the ionization gauge is operating or not, indicating that background atomic hydrogen from the gauge has a negligible influence on the measurements.

Figure 8 shows the influence of the temperature of the Pyrex glass reflector plate on the reflection of atomic hydrogen to the silicon crystal. Using the same

plate on the reflection of atomic hydrogen to the silicon crystal. Using the same method for evaluating relative efficiency as in Figure 7, we observe that the relative efficiency ratio  $\beta = 1.8 \pm 0.2$  for the Pyrex glass at 120 K and 300 K.

#### **IV. Discussion**

##### **A. The Recombination Coefficient of Atomic Hydrogen on Pyrex**

Several studies have demonstrated that the recombination coefficient for atomic hydrogen on Pyrex glass is in the range  $10^{-3}$  -  $10^{-4}$  for glass temperatures near 300 K [16]. In contrast, metal surfaces exhibit recombination coefficients above  $10^{-1}$  [16]. Thus, a Pyrex reflector surface was employed in this work to achieve almost total reflection of atomic hydrogen. The Pyrex reflector was cooled to 120 K in order to avoid the possible evolution of impurities from the glass due to incident atomic hydrogen, and also to avoid any effects of radiation heating of the Pyrex plate which also might liberate impurities.

Our measurements comparing the relative efficiencies of the two doser geometries (position 1 and position 2) to a calculation based upon apparatus geometry indicate that the recombination coefficient for atomic hydrogen on Pyrex is indeed small, making the reflector geometry efficient. Cooling to 120 K produces a more efficient atomic hydrogen reflection condition than at 300 K

##### **B. The Rate of Atomic Hydrogen Production on Tungsten**

The production of atomic hydrogen on hot tungsten has been studied extensively by others [4-6]. In a careful study done under high vacuum, but not ultrahigh vacuum conditions, Brennan and Fletcher [5] showed that for  $H_2$

proportional to the pressure of H<sub>2</sub>. At higher pressures, the rate becomes proportional to (P<sub>H<sub>2</sub></sub>)<sup>1/2</sup> at W filament temperatures near 1800 K. Their work showed that the activation energy for the atomization process on W was 52.9 ± 1.0 kcal/g. atom. Smith and Fite [4] showed that the efficiency of H atom production per H<sub>2</sub> collision on W increased from 0.1-0.3 in the temperature range 2200-2600 K, and then leveled off. Hickmott [6] reported a lower value for the efficiency of atomization of 0.05 above 1475 K, while Brennan and Fletcher [5] measured 0.25 for this efficiency and argued that the true value may be unity. All of this work, except for that of Hickmott, was done under conditions where contamination of the W sources by oxygen [4] or by hydrocarbons [5] was reported, so that the values obtained may not be characteristic of clean W.

The work of Hickmott [6] was carried out under ultrahigh vacuum conditions, using a W filament source for atomic hydrogen. An activation energy of 67 kcal/g·atom was measured for the atomization process. His W cleaning procedure consisted of flashing the filament to 2200 K in ultrahigh vacuum, after preliminary flashing to 3000 K to condition the filament.

In our work, checking the cleanliness of the tungsten surface by Auger spectroscopy was not possible. The W filaments used here have been heated occasionally to 2500 K in ultrahigh vacuum for cleaning, but were normally flashed only to 2000 K prior to each measurement. Thus, the kinetics of H atom production are characteristic of a working polycrystalline W surface like that which would often be employed in practice. This source produces atomic hydrogen at a rate which reaches a maximum near 2000 K. Similar results were reported by George et al. [17].

### **C. Comparison of H Atom Source Efficiency Using the Effusive Beam**

Figure 5 and Figure 7 show the kinetics of atomic hydrogen adsorption under conditions where the background pressure of H<sub>2</sub> is identical in the chamber [ $2 \times 10^{-7}$  Torr]. In Figure 5, a beam of H<sub>2</sub> causes a high density of H<sub>2</sub> to be present in the W filament region compared to the experiment shown in Figure 7. Comparison of the two curves in Figure 5 and Figure 7 at position 1 indicates that a factor of  $\sim 10$  increase in rate of atomic hydrogen adsorption is achieved when the beam doser is employed compared to a random gas flux. Thus using the beam doser results in a factor of  $\sim 10$  increase in atomic hydrogen adsorption, even with the decrease of a factor of  $\sim 5$  due to the geometrical limitation of the reflection geometry. In other words the beam doser produces a condition in which the gas density of H<sub>2</sub> and H at the W filament is  $\sim 50$  times greater than would be achieved with a random flux of H<sub>2</sub> produced by backfilling the chamber to achieve an identical H<sub>2</sub> pressure under dynamic pumping conditions.

### **D. The Advantages of the Reflector Atomic Hydrogen Beam Source**

The reflector atomic hydrogen beam doser described here has several advantages as listed below:

1. Minimal heating of the sample by radiation from the hot W filament.
2. Use of the source at high H<sub>2</sub> gas densities compared to those achievable by backfilling the chamber with H<sub>2</sub> under conditions of identical dynamic H<sub>2</sub> pressure conditions in the chamber.
3. Protection of the substrate from impurity species evolved by the W filament.

4. Production of only atomic hydrogen and  $H_2$  as compared to other sources involving electronic excitation of  $H_2$ .

## V. Acknowledgments

We acknowledge with thanks the support of the work by AFOSR under contract F49620-91-C-0032. KHB acknowledges BAFÖG financial support from the German government. We thank Dr. Jurgen A. Schaefer of the University of Kassel, Department of Physics for helpful assistance.

## References

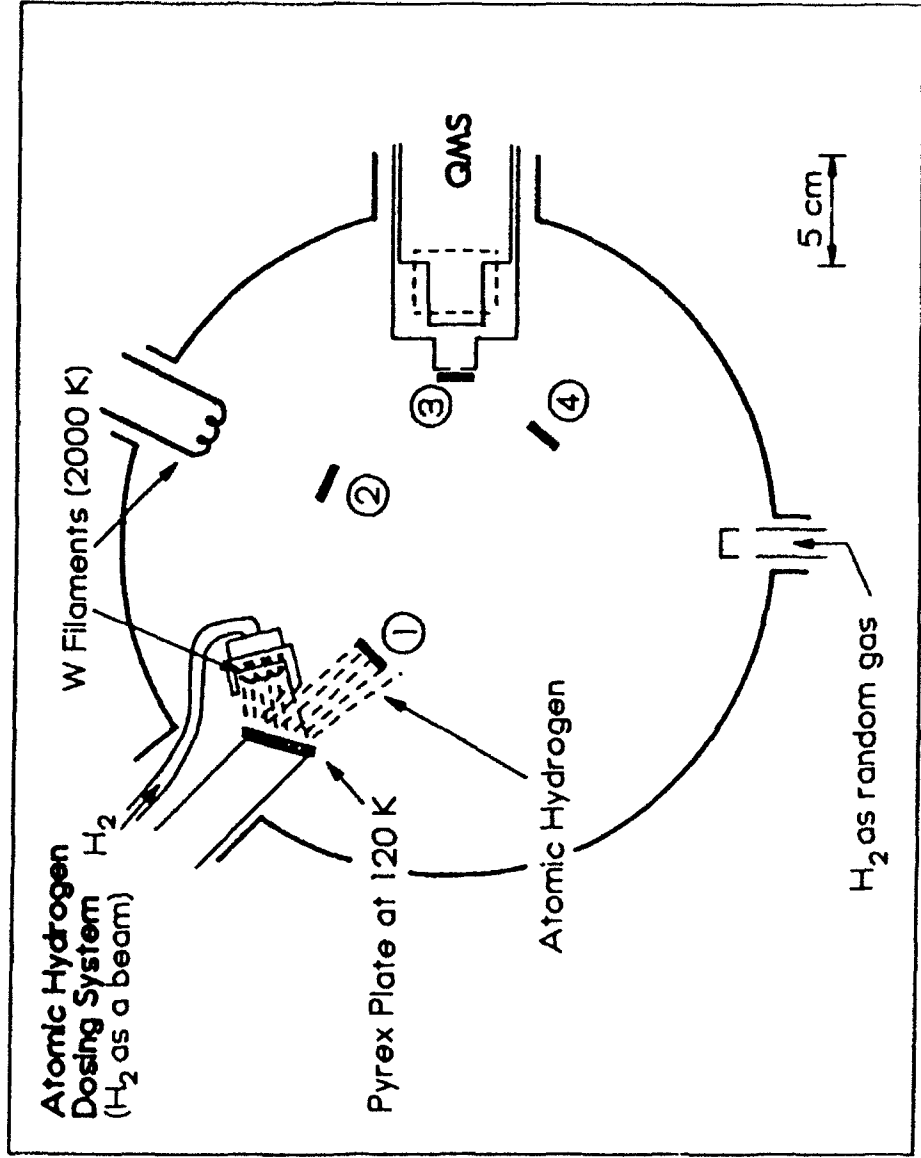
1. S.M. Rossnagel in "Thin Film Processes II," J.L. Vossen and W. Kern (Eds.), Academic Press, San Diego, 1991, chapter 1.
2. I. Langmuir, *J. Am. Chem. Soc.* 34, 1310 (1912).
3. I. Langmuir, *J. Am. Chem. Soc.* 37, 417 (1915).
4. J.N. Smith and W.L. Fite, *J. Chem. Phys.* 37, 898 (1962).
5. D. Brenna and P.C. Fletcher, *Proc. Roy. Soc. (London)* A250, 389 (1959).
6. T.W. Hickmott, *J. Chem. Phys.* 32, 810 (1960).
7. F. Rosebury, "Handbook of Electron Tube and Vacuum Techniques," Addison-Wesley, Massachusetts (1965), p. 80.
8. A. Winkler and J.T. Yates, Jr., *J. Vac. Sci. Tech.* A6, 2929 (1988).
9. A Roth, *Vacuum Technology* (2nd ed.), North-Holland, Amsterdam (1986), chapter 3.
10. W. Kern, *RCA Engineer* 28, 4, 99 (1983); *Semicond. Int.* April, 94 (1984).  
Modification of this procedure involved treatment of the crystal in NH<sub>3</sub>(aq) and HCl solutions to avoid nickel contamination.
11. M.J. Bozack, L. Muehlhoff, J.N. Russell, Jr., W.J. Choyke and J.T. Yates, Jr., *J. Vac. Sci. Tech.* A5, 1 (1987).
12. R.M. Wallace, P.A. Taylor, W.J. Choyke and J.T. Yates, Jr., *J. Appl. Phys.* 68, 3669 (1990).
13. C.C. Cheng and J.T. Yates, Jr., *Phys. Rev.* B43, 4041 (1991).
14. (a) K. Sinniah, M.G. Sherman, L.B. Lewis, W.H. Weinberg, J.T. Yates, Jr. and K.C. Janda, *J. Chem. Phys.*, 92, 5700 (1990); (b) J.A. Schaefer, *Physica* B170, 45-68 (1991).
15. Z.H. Lu, K. Griffiths, P.R. Norton and T.K. Sham, *Phys. Rev. Lett.* 68, 1343 (1992).

16. B.J. Wood and H. Wise, *J. Chem. Phys.* 29, 1416 (1958).
17. B.G. Koehler, C.H. Mak, D.A. Arthur, P.A. Coon and S.M. George, *J. Chem. Phys.* 89, 1709 (1988).

## Figure Captions

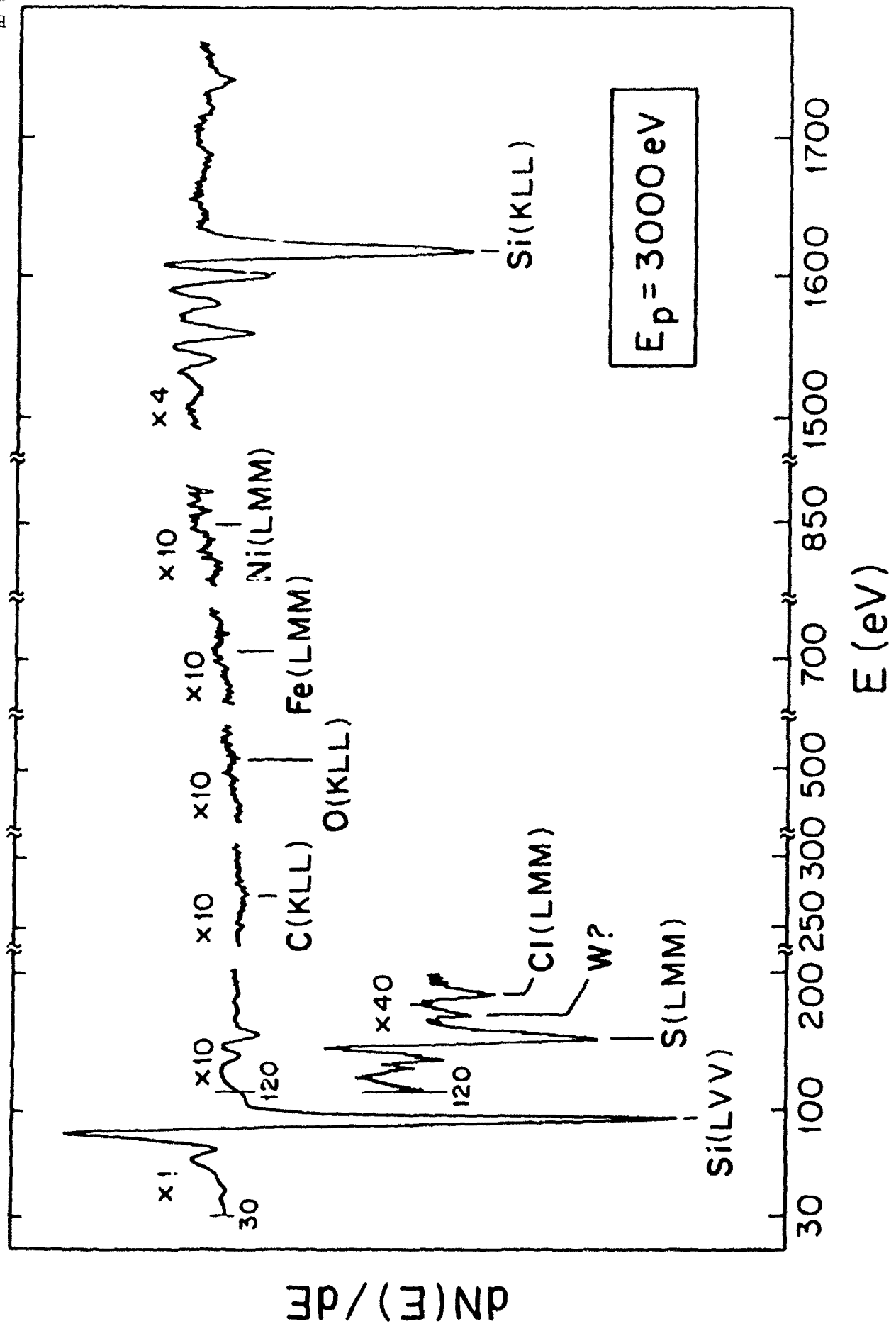
- Figure 1. The arrangement of the instruments and the four different crystal positions. Not shown are AES and RV LEED facilities.
- Figure 2. Auger spectrum of Si(100) after atomic hydrogen exposure and thermal desorption.
- Figure 3. The heating effect on the silicon crystal by reflected radiation from the reflector source.
- Figure 4. Thermal desorption spectra of H<sub>2</sub> from Si(100) for varying atomic hydrogen exposures.
- Figure 5. Development of hydrogen coverage on Si(100) for increasing exposure time using reflector hydrogen beam source.
- Figure 6. Efficiency of atomic hydrogen production on the tungsten filament as a function of tungsten temperature.
- Figure 7. Comparison of rate of hydrogen coverage increase between line-of-sight (position 2) and reflector source (position 1) using identical random fluxes of hydrogen onto the W filaments.
- Figure 8. Effect of Pyrex plate temperature on the rate of hydrogen coverage increase.

# CRYSTAL POSITIONS DURING EXPERIMENTS IN UHV SYSTEM

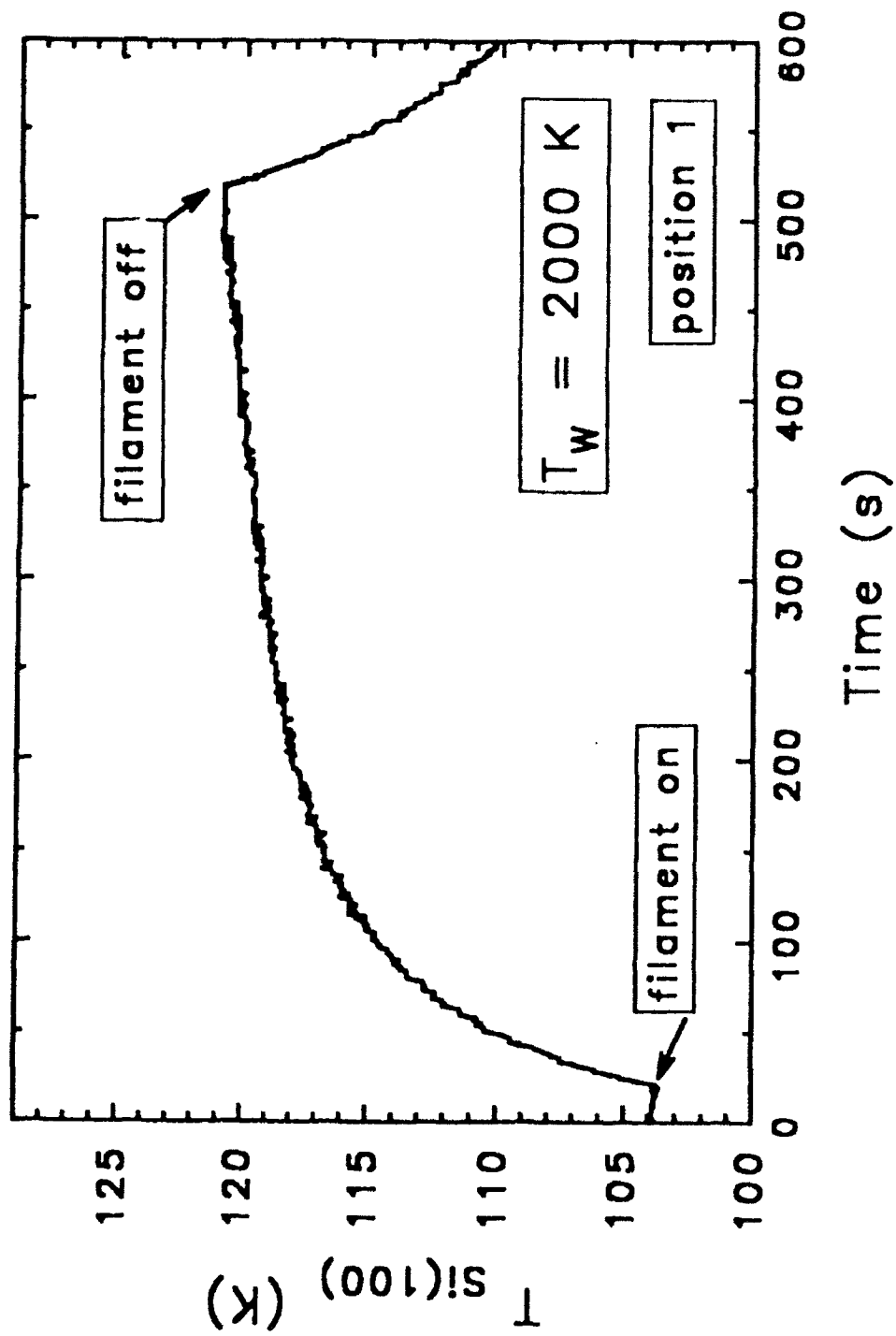


# Auger Electron Spectrum of a Clean Si(100) Surface

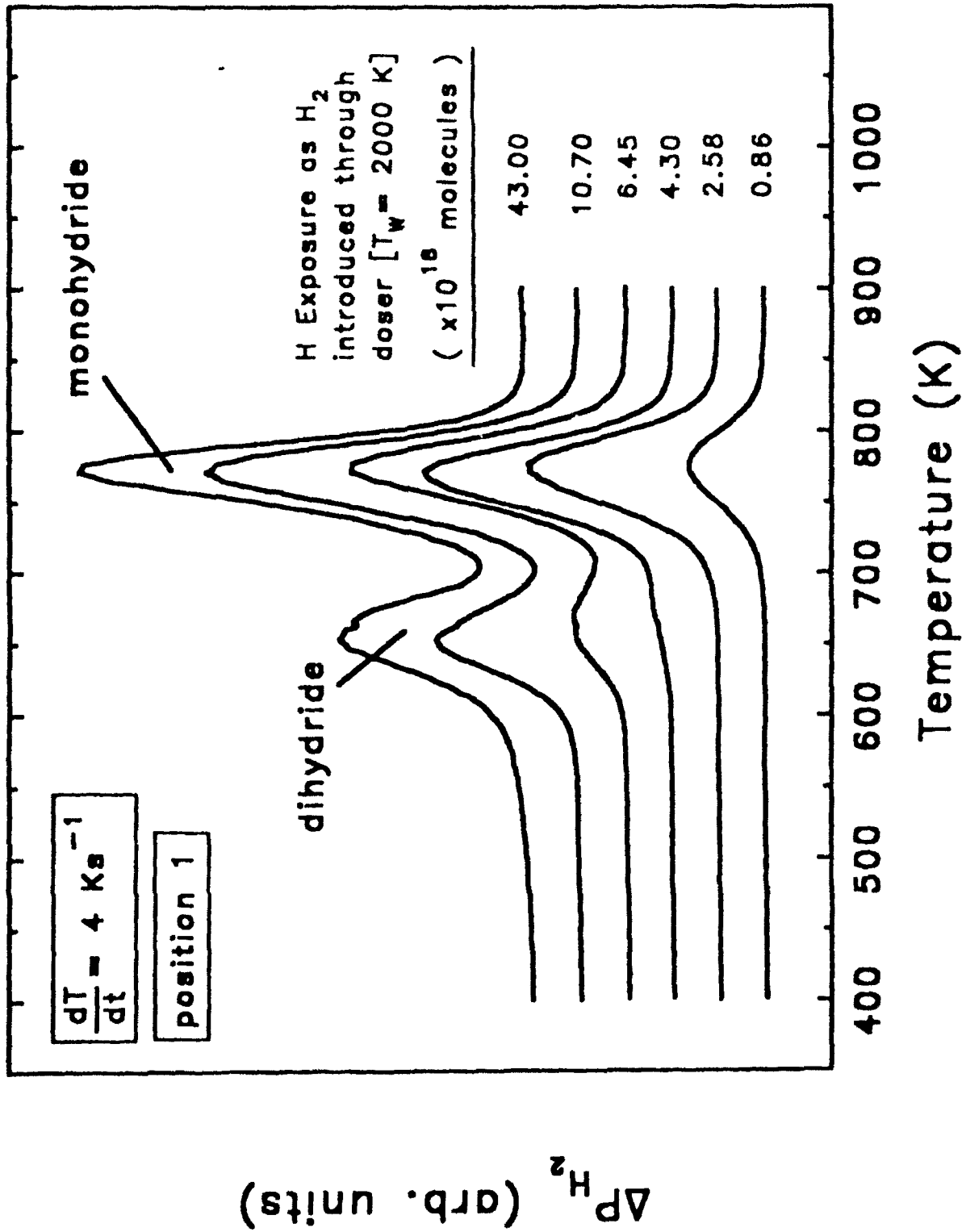
Bornscheuer, et al.  
Figure 2



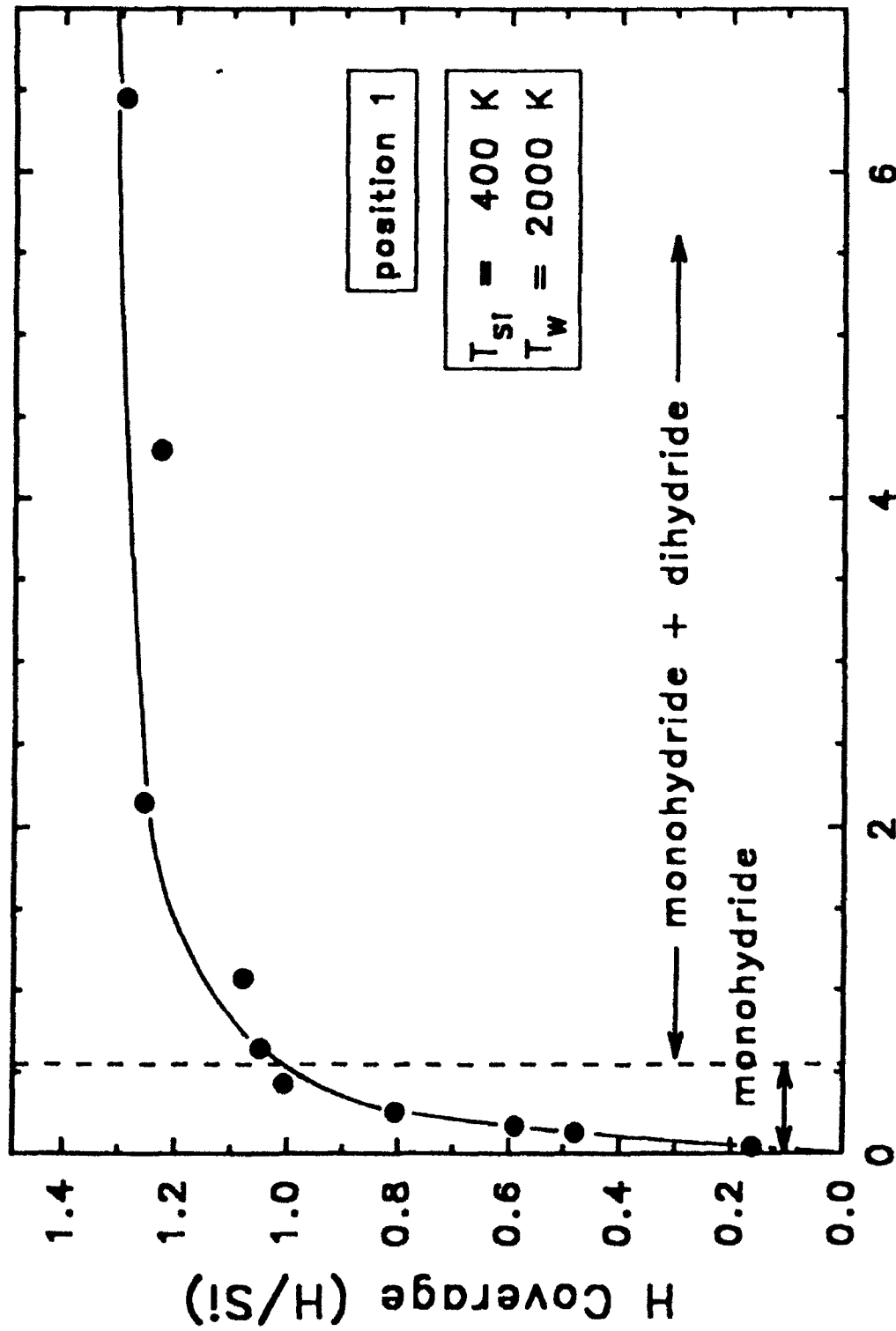
# CRYSTAL HEATING BY REFLECTED RADIATION



# TEMPERATURE PROGRAMMED DESORPTION: H/Si(100)



# DEVELOPMENT OF H COVERAGE ON Si(100) USING DIRECTED H<sub>2</sub> BEAM



H Exposure ( $\text{H}_2$  molecules introduced  $\times 10^{19}$ )

# EFFICIENCY OF ATOMIC HYDROGEN GENERATION ON TUNGSTEN FILAMENT

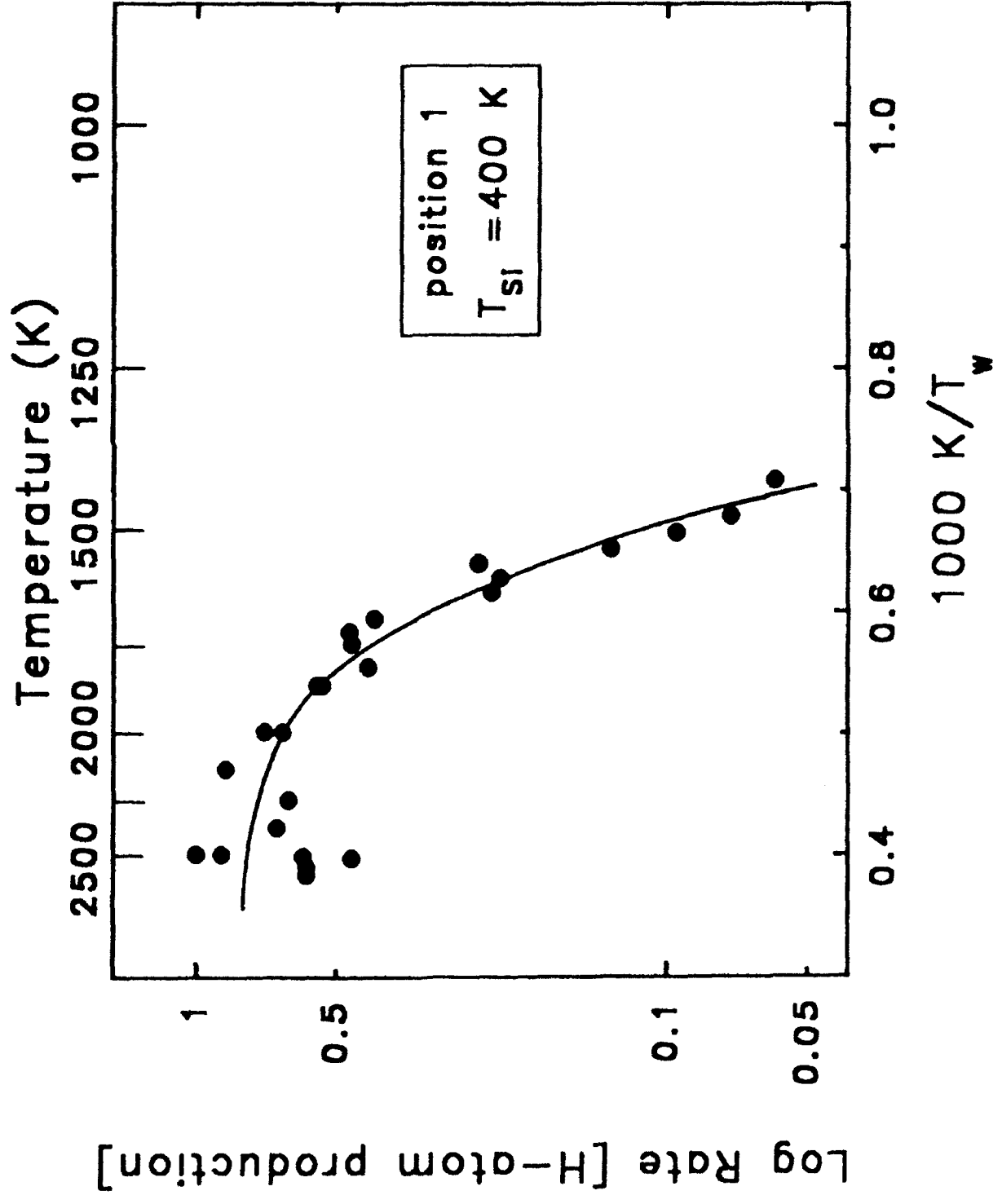
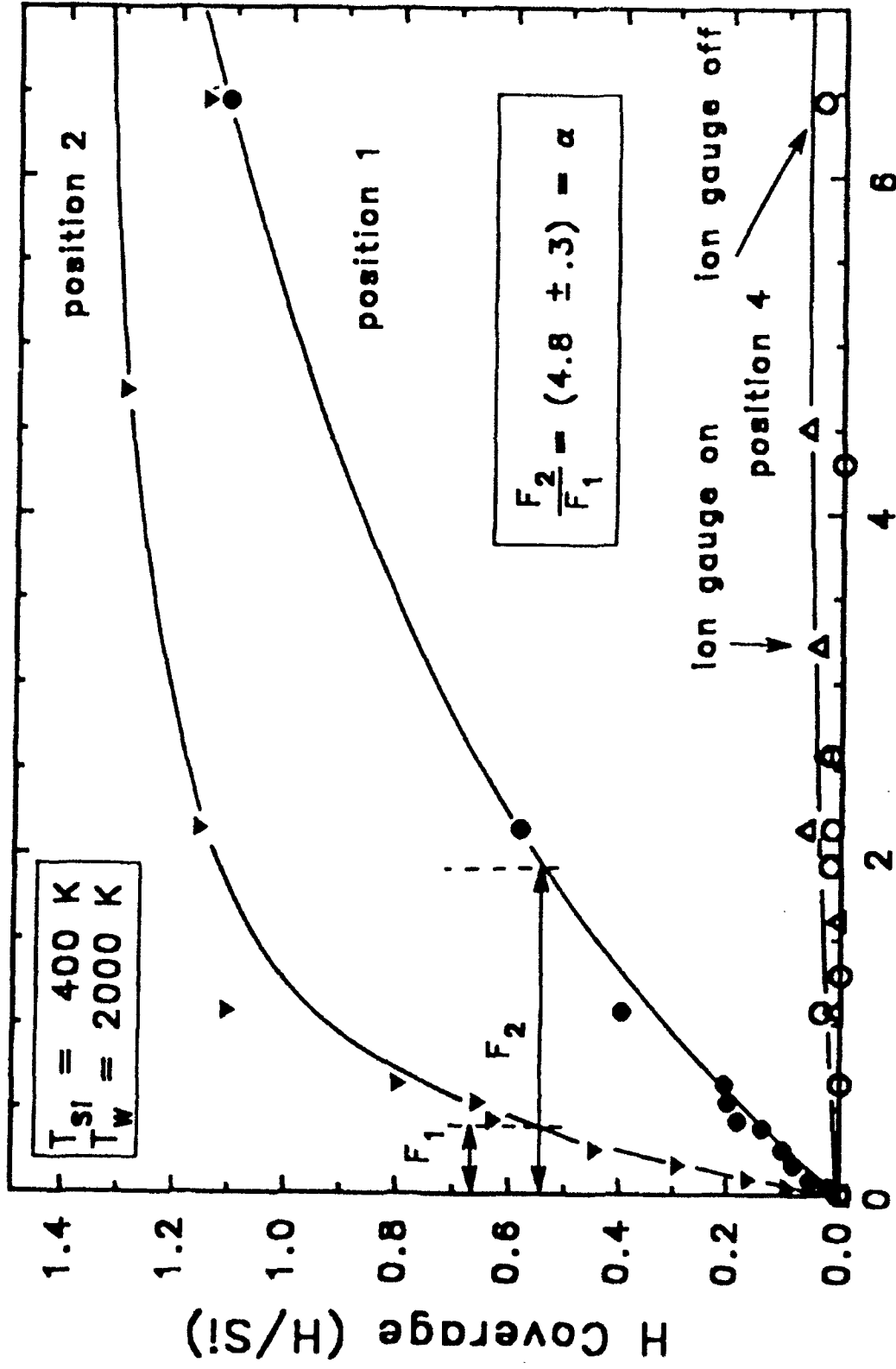


Figure 6

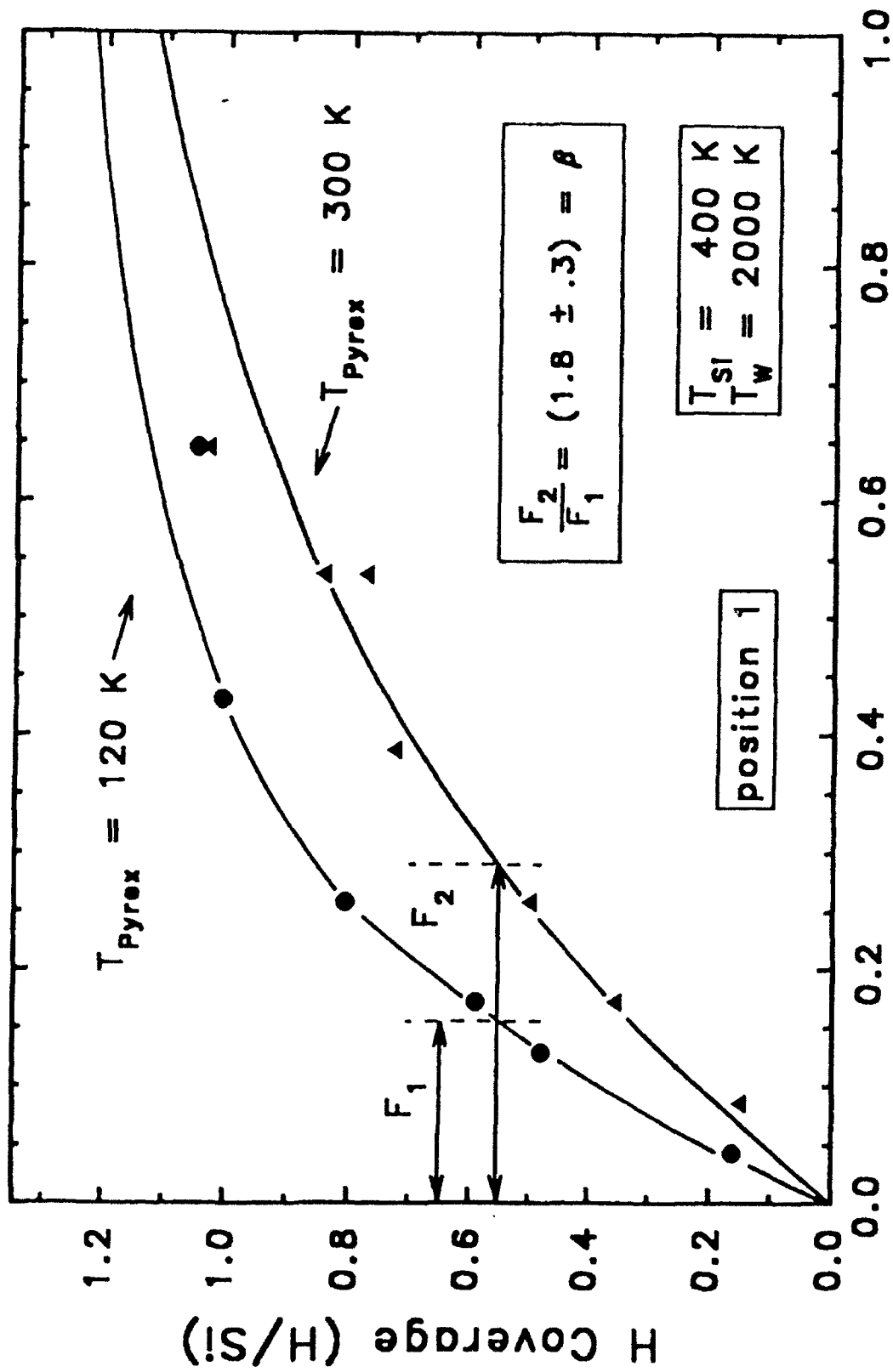
Bornscheuer,  
et al.

# COMPARING THE RATE OF ATOMIC H PRODUCTION USING RANDOM FLUX OF H<sub>2</sub>



H Exposure (H<sub>2</sub> molecules introduced x 10<sup>19</sup>)

# EFFECT OF PYREX REFLECTOR TEMPERATURE USING DIRECTED H<sub>2</sub> BEAM



H Exposure (H<sub>2</sub> molecules introduced × 10<sup>19</sup>)

**APPENDIX 2:**

M. F. MacMillan, R. P. Devaty, and W. J. Choyke, "Infrared Reflectance of Thin Aluminum Nitride Films on Various Substrates", Applied Physics Letters 62, 750 (1993).

# Infrared reflectance of thin aluminum nitride films on various substrates

M. F. MacMillan, R. P. Devaty, and W. J. Choyke

Department of Physics and Astronomy, University of Pittsburgh, Pittsburgh, Pennsylvania 15260

(Received 31 August 1992; accepted for publication 29 November 1992)

The measured room-temperature infrared reflectance at near-normal incidence of thin AlN films deposited by metalorganic chemical vapor deposition on various substrates is compared with calculated spectra based on Lorentz oscillator models for the reststrahl regions with parameters obtained from the literature. The effects of film and substrate anisotropy and non-normal incidence are included. The contribution of AlN can be analyzed even when the substrate and/or a thin overlayer have overlapping reflection bands. It is possible to obtain information on the thickness and other properties of the AlN films.

AlN is a wide band gap semiconductor of current interest for applications in optoelectronics.<sup>1</sup> Progress in the growth of high quality films requires the rapid characterization of samples. In this letter, we show that the room-temperature (RT) infrared (IR) reflectance measured by Fourier transform spectroscopy, when interpreted using simple models based on measured bulk parameters, provides information on the identity and quality of thin AlN films on various substrates. The contribution of the AlN can be extracted from a complicated spectrum even when the substrate has overlapping reststrahl bands.

The AlN films were grown by metalorganic chemical vapor deposition on Si and SiC substrates at Howard University. Film thicknesses were determined by profilometry. The orientations of most of the films were not measured. In general, the back surfaces of the substrates were not polished.

RT reflectance spectra were measured at 1 cm<sup>-1</sup> resolution on a Nicolet System 740 Fourier-transform infrared spectrometer using a KBr beamsplitter and a deuterated triglycine sulfate (DTGS) detector. The Spectra Tech Model 500 reflectometer was set at 5°, near normal incidence. The reflectometer makes use of a converging incident beam. The effect of the solid angle was estimated by calculating an rms average angle of incidence, 7.2°. A Pt film deposited on a polished sapphire substrate<sup>2</sup> was used as a reflectance standard. The spectra were not corrected for the reflectivity of Pt.

We model the IR properties of the films and substrates using Lorentz oscillators. There is disagreement regarding both the observation and assignment of lines in IR<sup>3-7</sup> and Raman<sup>8,9</sup> spectra of AlN. Therefore, we model AlN using an isotropic dielectric tensor. For a single oscillator, the frequency dependent complex dielectric function is

$$\epsilon(\omega) = \epsilon_{\infty} \left( 1 + \frac{\omega_L^2 - \omega_T^2}{\omega_T^2 - \omega^2 - i\gamma\omega} \right),$$

where  $\omega_T$  and  $\omega_L$  are the transverse and longitudinal optic mode frequencies, respectively,  $\gamma$  is the damping parameter, and  $\epsilon_{\infty}$  is the high frequency dielectric constant. The low frequency dielectric constant  $\epsilon_0$  is given by the Lyddane-Sachs-Teller relation  $\epsilon_0 = \epsilon_{\infty} \omega_L^2 / \omega_T^2$ . Table I lists the oscillator parameters. For AlN, we use the results of Akasaki and Hashimoto.<sup>4</sup> For 6H SiC, we use the param-

eters of Spitzer *et al.*,<sup>10</sup> with  $\epsilon_{\infty}$  as modified by Patrick and Choyke.<sup>11</sup> We use  $n = 3.42$  for the index of refraction of Si.<sup>12</sup>

We calculate the reflectance of absorbing anisotropic layers on substrates, which may be anisotropic and absorbing as well. The treatment of uniaxial films follows the method of Piro.<sup>13</sup> All uniaxial media are assumed to be oriented with their *c*-axes perpendicular to the surfaces and interfaces. In this case, the solution can be broken up into independent components with electric field vectors polarized either parallel (*p*) or perpendicular (*s*) to the plane of incidence. Both *s* and *p* polarizations are included, corresponding to unpolarized radiation. Complete account is taken of interference effects in the films. The best results are obtained when multiple reflections within the substrates are neglected.

Figures 1 and 2 show measured and calculated reflectance spectra for an AlN film deposited on a 0.02 cm thick Si substrate oriented 4° from (001). The film is polycrystalline, with a high degree of orientation. The Fabry-Pérot oscillations due to multiple reflections within the film are clearly visible in the transparent region of the spectrum above 1000 cm<sup>-1</sup> (Fig. 1). These data can be used to obtain the film thickness, given the index of refraction of AlN. The calculated curves in Fig. 1 were obtained by adjusting the thickness of the AlN film to 0.92 μm, which is in reasonable agreement with the 1.1 μm thickness measured by profilometry. One calculated curve includes the effect of multiple incoherent reflections within the substrate. For the other curve, we assume that the substrate is an infinite half-space. Clearly, neglect of multiple reflections within the substrate provides a better description of the data.

TABLE I. Oscillator parameters for AlN, 6H SiC

	$\epsilon_0$	$\epsilon_{\infty}$	$\omega_T$ (cm <sup>-1</sup> )	$\omega_L$ (cm <sup>-1</sup> )	$\gamma$ (cm <sup>-1</sup> )
AlN <sup>4</sup>	8.50	4.68	663.6	894.3	6.636
	8.50	4.68	663.6	894.3	6.636
SiC <sup>10</sup>	9.74	6.52	793.9	970.1	4.763
	10.07	6.70	785.9	959.7	5.501
			882.9	887.9	4.856

<sup>4</sup>Ref. 4

<sup>10</sup>Ref. 10, 11

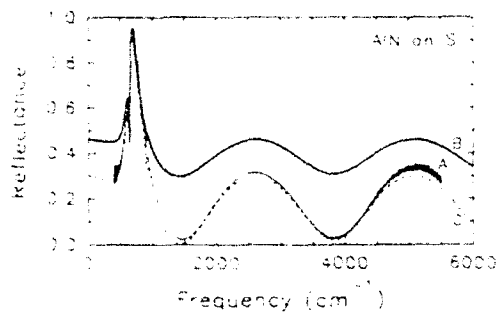


FIG. 1. Reflectance of 0.92  $\mu\text{m}$  thick AlN film on a Si substrate. A (solid line)—data; B (heavy solid line)—calculated spectrum, including multiple reflections within the substrate; C (dashed line)—calculated spectrum, neglecting multiple reflections within the substrate.

Figure 2 shows an expanded view of the AlN reststrahl region. Small oscillations due to multiple reflections within the substrate appearing in the data below  $550\text{ cm}^{-1}$  can be used to obtain the thickness of the substrate. Scattering at the substrate-air interface should decrease with decreasing frequency.

The model leads to the following interpretation of the reflectance spectrum. The large maximum is associated with the reststrahl of AlN. The two dips in reflectance near  $650\text{ cm}^{-1}$  are associated with absorption by the AlN  $\text{TO}(E_1)$  mode combined with interference effects. The dip at  $394.5\text{ cm}^{-1}$  is associated with the AlN  $\text{LO}(A_1)$  mode. It is observed at non-normal incidence for  $p$ -polarized radiation.<sup>14</sup>

There are two features in the data that are not explained by the model. First, there is a subsidiary maximum observed near  $610\text{ cm}^{-1}$ . This peak is larger for other samples. A mode near  $610\text{ cm}^{-1}$  was reported in IR and Raman studies on both single crystal and polycrystalline AlN, but there is disagreement on its assignment. Brafman *et al.*<sup>8</sup> observed a strong Raman line at  $610\text{ cm}^{-1}$  and interpreted its temperature dependence as an indication that it is not associated with a first-order Raman process. Pastrnak and Hejda<sup>5</sup> reported a line at  $610\text{ cm}^{-1}$  in IR transmission of needle-shaped crystals and related it to their assignment  $\omega_{\text{TO}}(A_1) \approx 621\text{ cm}^{-1}$ . They suggest that the  $610\text{ cm}^{-1}$  line is the  $E_1$  mode of a narrow cylinder,<sup>15</sup> which can be observed when the electric field is polarized parallel to the axis of the cylinder. Second, the dip near  $900\text{ cm}^{-1}$  is unexpectedly broad. A wurtzite crystal can have two distinct LO frequencies. The width of the measured

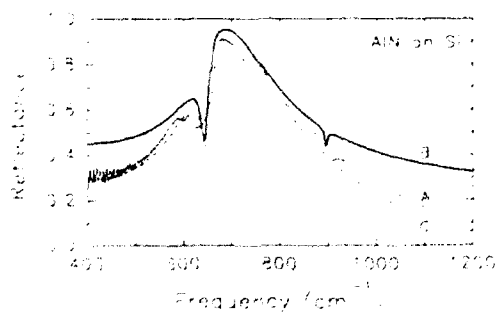


FIG. 2. Same as Fig. 1, expanded view of low frequency region

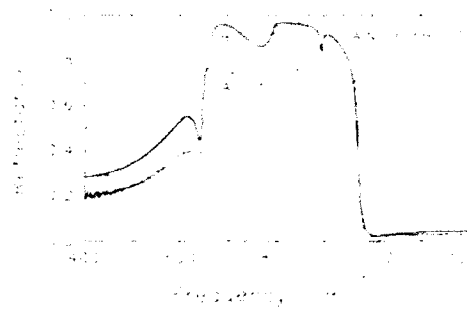


FIG. 3. Reflectance of 0.98  $\mu\text{m}$  thick AlN film on a (0001)-6H SiC substrate. A (thin solid line)—data; B (heavy solid line)—calculated spectrum, neglecting multiple reflections within the substrate; C (dashed line)—calculated spectrum, SiC substrate only

dip agrees with the difference between the LO frequencies measured by Sanjurjo *et al.*,<sup>9</sup> but their TO frequencies do not match our observations.

Figure 3 shows the IR reflectance for an AlN film on a (0001) face of a Lely grown 6H SiC substrate. Films prepared under similar growth conditions are known to be single crystal by electron channeling. The sample appears greenish, probably due to nitrogen impurities in the SiC. The film side is mostly specular. The back side is shiny but wavy, somewhat like crinkled Saran wrap, due to chemical etching. The film thickness determined by comparing measured and calculated Fabry-Pérot oscillations (not shown) is  $0.98\text{ }\mu\text{m}$ , which agrees very well with the value  $1\text{ }\mu\text{m}$  obtained by profilometry. But for the difference in intensity, the agreement between the measured and calculated spectra is good. Multiple reflections within the substrate are neglected. Also shown on Fig. 3 is the calculated spectrum for 6H SiC without an AlN layer. The high reflectance between  $800$  and  $990\text{ cm}^{-1}$  and the minimum near  $1000\text{ cm}^{-1}$  are associated with the reststrahl of the SiC substrate. The remaining features are associated with the AlN layer. The behavior between  $550$  and  $800\text{ cm}^{-1}$  is due to the  $\text{TO}(E_1)$  mode plus interference effects in the AlN film. There is no evidence for a mode at  $610\text{ cm}^{-1}$ . The dip near  $890\text{ cm}^{-1}$  is associated with the  $\text{LO}(A_1)$  mode of AlN, observable due to the non-normal incidence. For this sample, the dip is rather sharp, almost as sharp as the dip calculated from bulk parameters. There is no evidence for the  $\text{TO}(A_1)$  or  $\text{LO}(E_1)$  modes. The IR data indicate that this film may be of higher quality, or at least has a greater degree of  $c$ -axis orientation perpendicular to the surface. Note that the lattice mismatch between SiC and AlN is less than 1%. Using the observed dip in reflectance,  $\omega_{\text{LO}}(A_1) = 886.4\text{ cm}^{-1}$ , which is in agreement with Sanjurjo *et al.*'s<sup>9</sup> value of  $888 \pm 2\text{ cm}^{-1}$ .

Figure 4 shows the IR reflectance for a SiC film on an AlN epitaxial layer grown on a Si surface oriented  $4^\circ$  from (001). The SiC film is  $0.2\text{ }\mu\text{m}$  thick, based on the growth conditions. Fabry-Pérot oscillations within the cavity formed by the two films were observed at higher frequencies. Given the thickness of the SiC film, a  $0.6\text{ }\mu\text{m}$  thick AlN film provides the best match to the data. However, the calculated frequency of the minimum near  $730\text{ cm}^{-1}$ , which is an interference effect, did not match experiment.

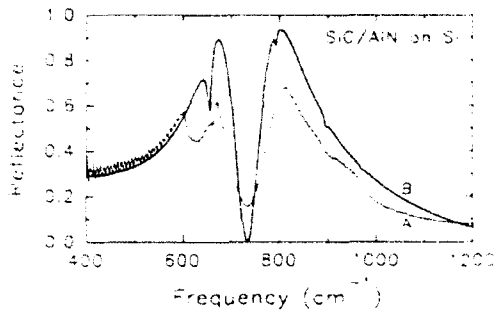


FIG. 4. Reflectance of  $0.24 \mu\text{m}$  SiC on  $0.56 \mu\text{m}$  AlN, deposited on a Si substrate. A (thin line)—data; B (thick line)—calculated spectrum, neglecting multiple reflections within the substrate.

By adjusting the thicknesses of both films while maintaining a constant total thickness, it is possible to match the minimum near  $730 \text{ cm}^{-1}$  while maintaining the agreement for the Fabry-Pérot fringes. According to our fit, the SiC film is  $0.24 \mu\text{m}$  thick and the AlN underlayer  $0.56 \mu\text{m}$ .

Based on the calculated spectrum (Fig. 4), the maxima near  $800 \text{ cm}^{-1}$  are associated with the  $\text{TO}_1$  mode in SiC (6H polytype assumed). The structure below  $700 \text{ cm}^{-1}$  is associated with the  $\text{TO}(E_1)$  mode of AlN. The dips in the calculated spectrum at  $656.5$ ,  $792.0$ ,  $694.5$ , and  $969.5 \text{ cm}^{-1}$  are due to absorption by the AlN  $\text{TO}(E_1)$ , 6H SiC  $\text{TO}_1$ , AlN  $\text{LO}(A_1)$ , and SiC  $\text{LO}_\parallel$  (the stronger of the two possibilities) modes, respectively. The TO frequencies are shifted from the model values due to the strong reflectance. The SiC  $\text{LO}_\parallel$  frequency does not match the value listed in Table I because the two modes of the  $c$ -axis component of the dielectric tensor  $\epsilon_{\parallel}(\omega)$  interact. The value of  $969.0 \text{ cm}^{-1}$  is obtained as one of the roots of  $\epsilon_{\parallel}(\omega) = 0$  for the parameters of Spitzer *et al.*,<sup>10</sup> ignoring damping. Once again, anomalous behavior is observed near  $600 \text{ cm}^{-1}$ .

We have shown that detailed information regarding anisotropic thin films can be obtained from reflection data in the reststrahl region and midinfrared by comparison with model calculations based on the assumptions that the bulk optical functions are known and described by Lorentz oscillators. For this method to be used most effectively as a diagnostic technique, there is a need for detailed infrared and Raman studies of bulk AlN as large single crystal samples become available.

The authors thank V. A. Dmitriev, K. J. Irvine, and M. G. Spencer (Howard University) for making available the samples used in this study. This research was supported by AFOSR Contract No. F49620 87 C 0101 through the Westinghouse Science and Technology Center (Subcontract No. 34 78382 PR).

- <sup>1</sup>R. F. Davis, Proc. IEEE **79**, 702 (1991)
- <sup>2</sup>J. V. Mantese, W. A. Curtin, and W. W. Webb, Phys. Rev. B **33**, 9897 (1986).
- <sup>3</sup>A. T. Collins, E. C. Lightowers, and P. J. Dean, Phys. Rev. **158**, 833 (1967).
- <sup>4</sup>I. Akasaki and M. Hashimoto, Solid State Commun. **5**, 851 (1967).
- <sup>5</sup>J. Pasternak and B. Hejda, Phys. Status Solidi **35**, 941 (1969).
- <sup>6</sup>J. Pasternak and B. Hejda, Phys. Lett. A **29**, 314 (1969).
- <sup>7</sup>C. Carlone, K. M. Lakin, and H. R. Shanks, J. Appl. Phys. **55**, 4010 (1984).
- <sup>8</sup>O. Brafman, G. Lengyel, S. S. Mitra, P. J. Gielisse, J. N. Plendl, and L. C. Mansur, Solid State Commun. **6**, 523 (1968).
- <sup>9</sup>J. A. Sanjurjo, E. Lopez-Cruz, P. Vogl, and M. Cardona, Phys. Rev. B **28**, 4579 (1983).
- <sup>10</sup>W. G. Spitzer, D. Kleinman, and D. Walsh, Phys. Rev. **113**, 127 (1959).
- <sup>11</sup>L. A. Patrick and W. J. Choyke, Phys. Rev. B **2**, 2255 (1970).
- <sup>12</sup>D. F. Edwards, in *Handbook of Optical Constants of Solids*, edited by E. D. Palik (Academic, Orlando, 1985), pp. 547-569.
- <sup>13</sup>P. Piro, Phys. Rev. B **36**, 3427 (1987).
- <sup>14</sup>D. W. Berreman, Phys. Rev. **130**, 2193 (1963).
- <sup>15</sup>R. Englman and R. Ruppin, J. Phys. C **1**, 1515 (1968); R. Ruppin and R. Englman, Rep. Prog. Phys. **33**, 149 (1970).